MM Science Journal | www.mmscience.eu
ISSN 1803-1269 (Print) | ISSN 1805-0476 (Online)
Special Issue | HSM 2023
17th International Conference on High Speed Machining
October 25-28, 2023, Nanjing, China
DOI: 10.17973/MMSJ.2023_11_2023118

HSM2023-00055

INFLUENCE OF HEAT TREATMENT AND DIFFERENT CUTTING CONDITIONS ON THE MACHINABILITY IN ADDITIVE-SUBTRACTIVE PROCESSING

J. Steiner-Stark[1]*, M. Zimmermann[1], J. Platz[1], B. Kirsch[1], J.C. Aurich[1]
[1]RPTU Kaiserslautern, Institute for Manufacturing Technology and Production Systems, Kaiserslautern, Germany
*Corresponding author; e-mail: johanna.steiner-stark@rptu.de

Abstract
For many applications, the surface quality, geometric accuracy and stress state of parts produced using laser-based powder bed fusion (PBF-LB) are insufficient. A stress relief and machining as post-processing operations allow to overcome these issues. PBF-LB materials have a unique microstructure. Their machinability therefore differs from that of cast or wrought materials. The microstructure can be altered by a stress relief heat treatment, which can change the machinability further.
In this paper, the machinability of AlSi10Mg parts in the as-built condition and stress relieved condition is examined when wet and dry peripheral milling with cutting speeds up to 1,000 m/min. The PBF-LB parts were manufactured in different build-up directions. The stress relief decreased the material microhardness by approximately 16 %. This lower microhardness did not significantly affect the process forces but influenced the surface characteristics. The best surface quality was achieved when milling with the highest considered cutting speed of 1,000 m/min and when using metalworking fluids. Particularly the number of surface defects such as the smearing of material could thus be reduced. For the as-built conditions, good surface qualities can be achieved in dry cutting with high cutting speeds.

Keywords:
Additive manufacturing, laser powder bed fusion (PBF-LB), stress relief heat treatment, high speed milling, post-processing

1 INTRODUCTION

Aluminium silicium alloys, like AlSi10Mg, are often used in in the automotive and aerospace industry due to their good mechanical properties, low density and low coefficient of thermal expansion [Read 2015] Additive manufacturing (AM) enables a high degree of freedom in design [Gebhardt 2013] and offers great potential for lightweight applications [Plocher 2019]. Due to the beneficial properties of AlSi10Mg for lightweight applications, this aluminum alloy is a key material for additive manufacturing. Laser-based powder bed fusion (PBF-LB) as an additive manufacturing process is used in numerous applications in industry. PBF-LB enables the production of metal parts with high densities and good mechanical properties [Aboulkhair 2019; Raus 2017; Wei 2017; Buchbinder 2013; Kempen 2012]. AlSi10Mg and other materials processed by PBF-LB show different material properties than conventionally manufactured (e. g. cast or wrought) materials. The layer-by-layer manufacturing principle and the high cooling rates of the material during PBF-LB lead to anisotropic part properties and a fine-grained material microstructure [Kempen 2012]. High residual stresses caused by high cooling rates and reheating cycles can cause part deformations [Wang 2018]. Those deformations and other geometrical inaccuracies combined with the low surface quality makes the quality of PBF-LB parts insufficient for many applications [Calignano 2017; Leary 2017]. To meet the specific part requirements several post-processing routes can be applied to PBF-LB parts, including different heat treatments [Fiocchi 2021] and different subtractive finishing processes [Malakizadi 2022].

For PBF-LB AlSi10Mg, different solution and ageing treatments, direct ageing and annealing heat treatments were studied concerning their impacts on the microstructure and mechanical properties [Fiocchi 2021]. Annealing can reduce the residual stresses and improve the ductility of PBF-LB parts [Maamoun 2018]. Our previous work has shown that annealing PBF-LB AlSi10Mg parts can reduce their deformation after the removal from the build platform by up to 450 % [Schmidt 2022].

Machining as a post-processing technique can improve both the geometrical accuracy and the surface roughness [Oliveira 2021; Milton 2016]. Several studies revealed

differences in the machinability of PBF-LB materials and cast materials [Brinksmeier 2010; Neuenfeldt 2021; Alexeev 2017; Fernandez-Zelaia 2019; Bai 2021; Milton 2016; Pérez-Ruiz 2021; Jarosz 2020; Ming 2019]. These differences were explained by the different microstructures and mechanical properties. Moreover, the process-related anisotropy of LBF-PF materials also influences the machining. Differences in forces and surface qualities were reported when machining parallel or perpendicular in relation to the build-up direction [Fernandez-Zelaia 2019; Pérez-Ruiz 2021; Jarosz 2020]. [Bai 2021] and [Fortunato 2018] observed changes in the forces, surface characteristics and tool wear when milling heat-treated parts made of steel in comparison to the as-built parts. This was attributed to the microstructural changes caused by the heat treatment.

Although AlSi10Mg has been widely studied concerning PBF-LB processing and material properties, there are only a few studies addressing the machinability of PBF-LB AlSi10Mg. [Segebade 2019] performed orthogonal cutting with parts manufactured in three different build-up directions. They observed differences in the specific cutting forces and the chip ratio in dependence on the direction of feed travel of the tool in relation to the build-up direction. They explained the differences with the alignment of the layers in relation to the primary shear zone. [Piscopo 2019] studied face milling of stress relived PBF-LB parts and cast AlSi10Mg parts. The process forces were lower for the PBF-LB parts. The smaller process forces also led to lower machining induced compressive stresses in the PBF-LB parts. [Ramoni 2021] compared different cooling strategies (dry, wet and minimal quantum lubrication) in face milling. The surface topography of all samples was characterized by a flaky structure, which was most pronounced when dry milling. We [Zimmermann 2021] observed a similar surface structure after dry milling of AlSi10Mg PBF-LB parts. A comparison with cast material revealed differences in the resultant force, chip form and surface quality. Moreover, these results varied with regard to the PBF-LB process parameters and the feed travel in relation to the build-up direction of the parts.

In the studies presented, only low cutting speeds up to 380 m/min were investigated for the machining of additively manufactured aluminum alloys [Piscopo 2019]. However, high cutting speeds can allow for two decisive improvements: the time needed for machining can be significantly reduced and the surface quality might also be improved. For conventionally manufactured Al-Si alloys, machining with high cutting speeds is applicable and has improved the surface qualities in some cases [Santos 2016]. In this study, milling with cutting speeds up to 1,000 m/min is investigated as a finishing process for as-built and stress-relieved PBF-LB AlSi10Mg parts. Moreover, the influences of the build-up direction and cooling condition (flood cooling and dry) on the process forces and the surface properties are explored.

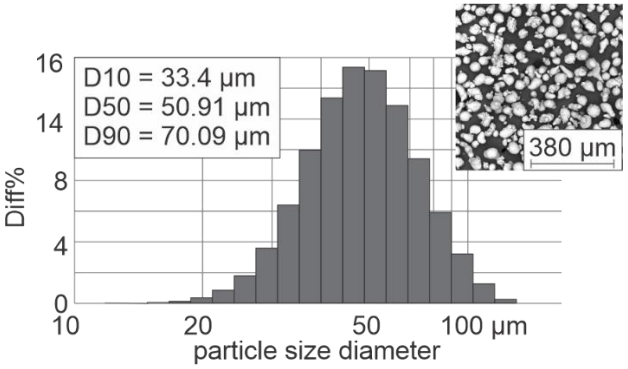

Figure 1: Particle size distribution and SEM image of powder particles

2 EXPERIMENTS

2.1 Additive manufacturing

The parts were fabricated on the PBF-LB machine ProXDMP320 from 3D Systems[1]. The powder size distribution of the AlSi10Mg powder used was measured using the Bettersize S3 Plus particle analyzer from 3P Instruments[1]. The powder size distribution and morphology are shown in Figure 1. The process parameters used for the PBF-LB and the powder size distribution is listed in Table 1. The inert process atmosphere during the PBF-LB was realized via argon. The build platform was not heated. The parts were built in two directions in relation to the build platform. The part geometry and part orientation (0° and 45°) can be found in Figure 2. The density of the parts was determined according to the Archimedes' principle. The weight of three parts of each build-up direction was measured in air and in distilled water ($\delta_{water\_20°C}$ = 0.9982 g/cm³) with a precision balance (Kern EMB-V 200-3V[1]). The relative density was calculated by comparing the measured density and the theoretical density ($\delta_{AlSi10Mg}$ = 2.68 g/cm³) as specified by the powder supplier 3D Systems[1]. The parts showed a relative density of 99.47 ± 0.43 %. The build-up direction did not influence the relative density.

Table 1: PBF-LB process parameters and powder size distribution

laser power	250 W
scanning speed	1,300 mm/s
layer thickness	30 µm
hatching distance	90 µm
scanning strategy	Bi-directional stripes, rotation of 245° after each layer
laser spot diameter	80 µm
fiber laser wavelength	1070 nm

Half of the parts were heat treated using the stress relief annealing that was also used in our previous work [Schmidt 2022]. The parts were heated up to 300 °C with a heating rate of 1 °C/min. The peak temperature was held for 2 hours. After that, the parts were cooled to room temperature

in the air. The as-built parts are labled as AB and the heat-treated parts as HT.

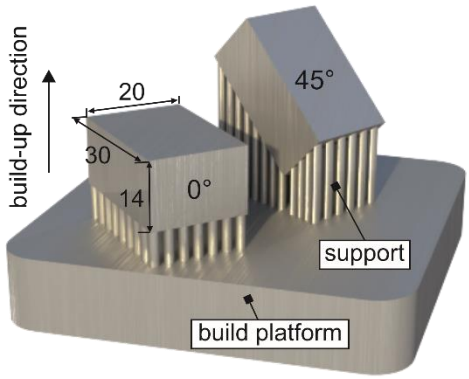

Figure 2: Part geometry and different orientations on build platform

2.2 Milling

The milling was performed on the 5-axis machining center Röders RXP601DSHZ2[1]. The experimental setup is shown in Figure 3. The parts were machined in a peripheral down milling operation with an axial and radial depth of cut of a_p = 5 mm and a_e = 0.4 mm, respectively. The feed per tooth was constant (f_z = 0.06 mm). Cutting speeds of v_{c1} = 500 m/min and v_{c2} = 1,000 m/min were used for milling except for the parts AB 45° and HT 45°. These were milled with v_{c2} = 1,000 m/min only. Milling was carried out both with flood cooling (wet) and dry. For the flood cooling, the grinding oil DiaMond100 from Oelheld[1] was supplied with a total volume flow of 27 L/min through six nozzles mounted on the spindle. The tool used was an uncoated three tooth cemented carbide end mill (Gühring Alu RF A[1]) with a diameter of 10 mm. A new tool was used after seven cuts. This number of cuts was defined on the basis of preliminary tests. In the preliminary tests, no significant signs of wear were found on the tools after 7 cuts (these correspond to a feed travel of 210 mm). The trials were executed randomized to limit the influence of tool wear on the results. Each of the different experiments was carried out three times.

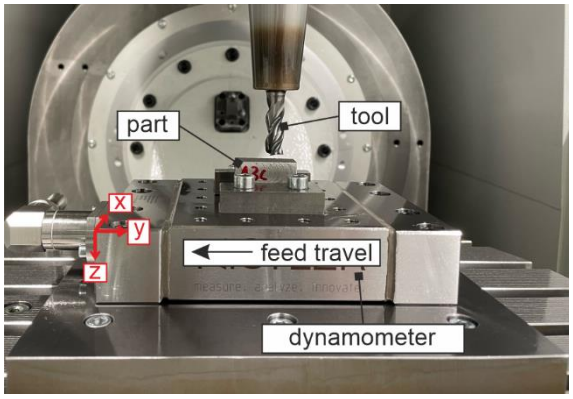

Figure 3: Experimental set-up for milling

2.3 Characterization

Sections of the as-built parts and heat treated parts were made perpendicuar to the feed travel of the end mill for both part orientations (see Figure 4). The surfaces of the sections were etched with Keller's etching agent (2.5 % nitric acid HNO3, 1.5 % hydro-chloric acid HCl, 1 % hydrofluoric acid HF, rest water) for 15 sec to reveal the microstructure, which was investigated under a light microscope.

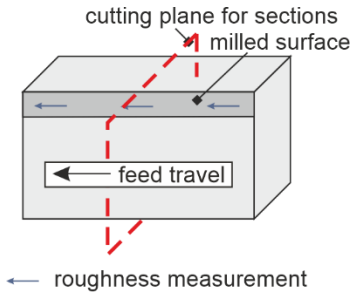

Figure 4: Orientation of sections for microstructural characterization and positions for the roughness measurements

The microhardness was measured with the MicroMet 5100 tester from Buehler GmBH[1] using a Vickers indenter. Nine measurements with a load force of 100 gf were carried out on each section (measured according to DIN EN ISO 6507-1:2018). The mean value was calculated from these nine measurements. The positions of the individual measurements were the same for all the parts.

The surface roughness was measured with a stylus instrument (MarSurf XR20 GD120[1]) in the direction of feed motion of the end mill. Three measurements with a respective measuring length of 5.6 mm were performed on each machined surface. Measurements were carried out at approximately the same locations for each machined part. The locations are depicted in Figure 4. A cut-off wavelength λ_c of 0.8 mm was used to eliminate the waviness from the roughness calculation. The surface roughness of the as-built parts AB 0° and AB 45° was measured analogously. The surface roughness parameter arithmetic mean roughness R_a and the average maximum height R_z were calculated according to DIN EN ISO 4287:2010. Images of the as-built surfaces and machined surfaces were captured with a scanning electron microscope (SEM, FEI Quanta 600 FEG[1]).

During milling, the process forces were measured with a Kistler 9129AA[1] dynamometer and a sampling rate of 100 kHz. After the data acquisition, the force data was filtered with a least-square linear filter (f_{pass} = 1.9 kHz and f_{stop} = 2.3 kHz). For the evaluation of the forces, 10 % of the signal was cut off at the beginning and the end to exclude the data from the non-stationary tool engagement (tool entrance and tool exit) from the evaluation. For wet milling, the forces in x- and y-direction generated by the impact of the metalworking fluid on the dynamometer were subtracted from the force data measured during milling. To determine these offsets, the forces generated by the metalworking fluid impact on the dynamometer were measured without a tool engagement. To evaluate the forces, the maximum active force F_a was calculated:

$$F_a = \sqrt{\bar{F}_{x\_peak}^2 + \bar{F}_{y\_peak}^2}$$

The forces F_{x_peak} and F_{y_peak} represent the maximum forces during the tooth engagements in x- and y-direction, respectively. The maximum forces were determined for each tooth engagement. The average of these maximum forces was calculated to determine the active forces.

3 RESULTS AND DISCUSSION

3.1 Microstructure and microhardness of the parts

The microstructure of the as-built parts exhibits the process related 'fish scale' pattern, typical for PBF-LB parts (see Figure 5). This pattern results from the building principle. Numerous laser scan paths are lined up in each layer to build the part. At each laser scan path, a melt border is formed during the solidification of the material. This generates a scale pattern. The images show different scale patterns for a 0° and 45° built-up direction. In the case of the 45° built-up direction, the melt path features are more irregular. The heat treatment partially dissolved the characteristic melt path borders for both build-up directions. They are less clearly visible but still present.

The microhardness of the as-built parts and heat-treated parts is shown in Figure 6. The microhardness in both built-up directions considered is approximately the same. Consequently, there is no influence of the build-up direction on the microhardness. The heat treatment significantly reduces the materials microhardness by about 16 %. This finding is in good agreement with other studies [Růžičková 2022; Uzan 2017]. One of the main reasons for the high hardness of AB AlSi10Mg parts is a continuous Si-network that encloses the α-aluminum. This Si-network forms a barrier for dislocation movement and strengthens the material. During annealing, the Si-network starts to segregate into discontinuous Si-particles, and the strengthening mechanism present for the AB microstructure is weakened. [Růžičková 2022] The standard deviations of the microhardness values are slightly lower for the heat treated parts. This indicates a more homogeneous microstructure after the heat treatment.

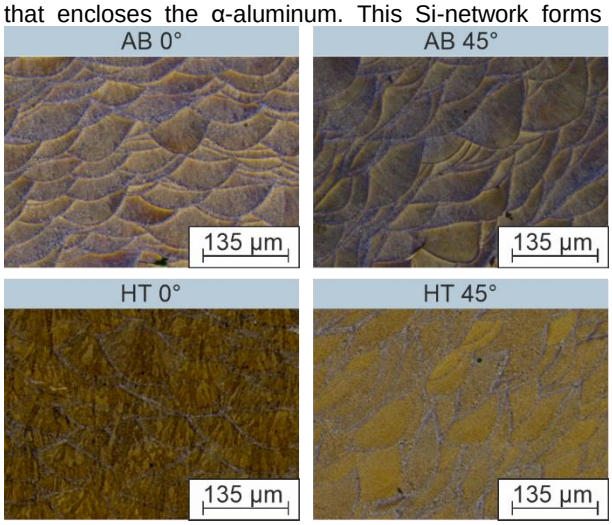

Figure 5: Microstructure of as-built and heat-treated PBF-LB materials

3.2 Process forces during milling

The active forces during the different milling conditions are shown in Figure 7**.** Under flood cooling, the forces of the HT 0° parts are lower than for the AB 0° parts. This could be explained with the higher hardness of the AB parts. A higher hardness of the material leads to a higher resistance against plastic deformation, in this case against the chip formation during the cutting process. For the heat treated parts, the active force can be effectively reduced by using metalworking fluid. This finding is in good agreement with other studies investigating the machining of aluminum alloys [Sreejith 2008; Kishawy 2005]. The lower active forces in wet milling can be explained with the lubrication properties of the metalworking fluid and the resulting reduction in friction between the tool and material. For the lower cutting speed of 500 m/min the decrease of the active force is more pronounced than for the higher cutting speed. The effectiveness of the coolant lubrication might be smaller at the higher cutting speed because the metalworking fluid cannot penetrate the contact as well as for the cutting speed. [Grzesik 2019] assumed that higher rational speeds of the tool limit the lubrication of the cutting edge with the metalworking fluid. For the AB 0° material, there is no significant influence of the metalworking fluid on the active forces. The AB 0° material is more brittle than the HT material and the effectiveness of the application of

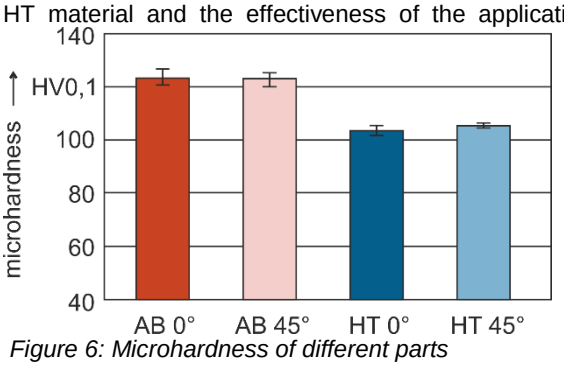

Figure 6: Microhardness of different parts

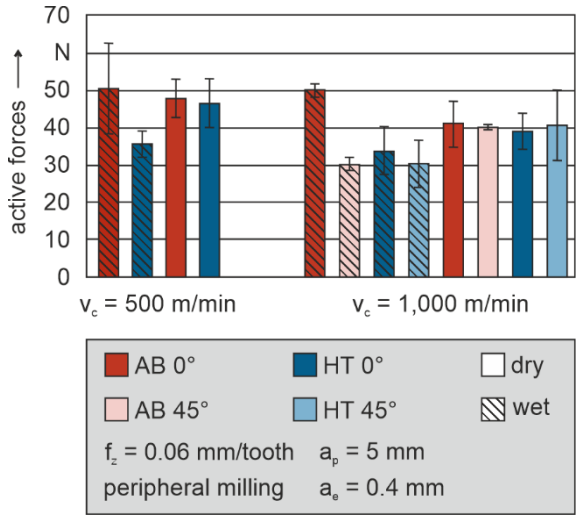

Figure 7: Active forces

metalworking fluid is reduced. This might be due to a smaller tool/chip contact area when machining a more brittle material. Because of the smaller contact area, the friction between tool and chip is generally smaller. A reduction of this friction with the use of metalworking fluids therefore has a smaller overall impact on the process forces.

An increase in cutting speed decreases the active forces. This can be attributed to the increasing material temperature in the shear zones and the resulting reduction of the flow stress. Another mechanism that contributes to the lower forces is the smaller tool/chip contact area at higher cutting speeds. The smaller contact area reduces the friction work to be done on the rake face [Rao 2001]. The extent of the effect of the cutting speed on the forces depends on the cooling lubrication condition used. In dry machining, we found a greater influence of the cutting speed on the active forces than in wet machining. [Zedan 2013] and [Ozcelik 2011] also observed a smaller influence of the cutting speed on the process forces when metalworking fluid is applied. We believe that this is due to the generally significantly lower material temperatures in

this case. An increase of the cutting speed therefore results in a smaller temperature rise of the material.

For dry milling, there is no significant influence of the build-up direction on the active forces. For flood cooling, however, the active forces of the AB parts built in 0° direction are higher than for the AB 45° parts. This effect was not observed when milling the heat-treated parts. This indicates that the heat treatment reduces the anisotropy of the materials microstructure.

3.3 Surface quality

The surface roughness parameters R_a and R_z of the as-built surfaces and the milled surfaces are presented in Figure 8. In AB conditions, the surface roughness of parts built in 45° build-up direction is higher than for parts built in 0° build up direction. These differences can be explained by the surface characteristics, as shown by the SEM images in Figure 9. The surface of the AB 0° parts exhibits a structure similar to laser welding seams. In addition, small spherical particles are clearly visible. They could be caused by material ejected from the melt pool, which then sticks to the surface. The surface of the AB 45° part is mainly characterized by powder particles. These originate from the surrounding powder bed in 45° built-up direction. The surrounding powder bed is heated and nearby powder particles were partially melted during PBF-LB and therefore adhere to the surface

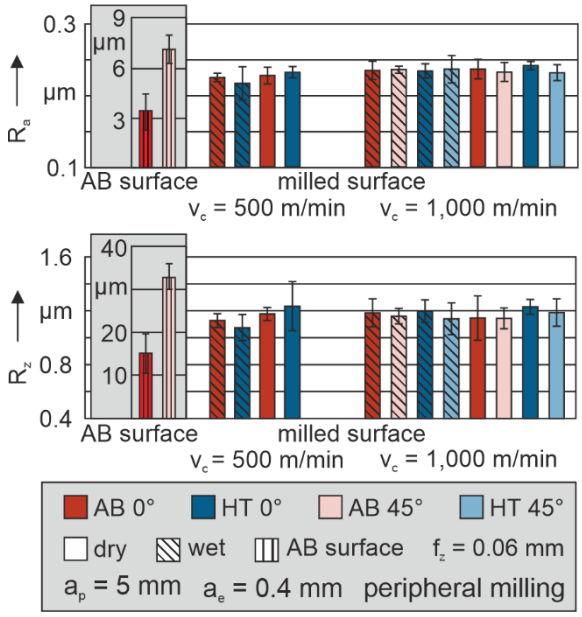

Figure 8: Measured surface roughness parameters

Milling improved the surface roughness of the PBF-LB parts significantly. The cutting conditions considered did not significantly affect the surface roughness. Therefore, it can be concluded that the kinematic roughness resulting from the movement of the cutting edges through the material is decisive for the measured values of the surface roughness. The kinematic roughness represents the theoretically achievable roughness. The theoretical mean roughness R_{zt} can be approximated as $R_{zt} = f_z^2/(4 * d)$. With the parameters used in this study, the theoretical roughness value equals to R_{zt} = 0.09 µm. The determined R_z values are significantly higher. This can indicate tool-runout errors which lead to higher surface roughness parameter values. This assumption is supported by the surface profiles.

A representative profile for the measured surface topographies is presented in Figure 10. Theoretically, the peaks in the profile are one feed per tooth apart (i.e. 0.06 mm). The peaks of the measured surface profiles are about 0.18 mm apart, which equals to 3*f_z. When modelling the kinematics in peripheral milling, as suggested in [Krüger 2014], a radius deviation of just 1 µm of one tooth leads to the same phenomenon in the surface profile as we have observed. To prove the existence of such a tool runout error, the differences in tooth radii were measured using a dial gauge for 10 tools clamped in the spindle. The differences between the tooth radii were between 2 and 8 µm. Consequently, the kinematic roughness is caused by the movement of just one of the three tooth and larger surface roughness values are generated.

SEM images were used to investigate potential geometrical surface irregularities. Surface pores were found on the milled surfaces (see Figure 11).

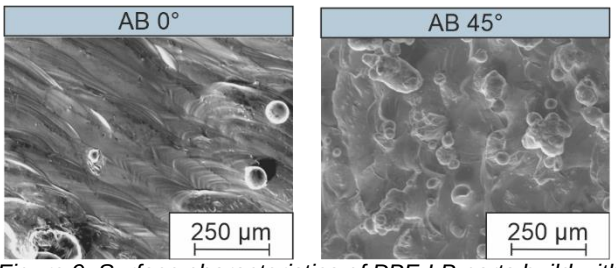

Figure 9: Surface characteristics of PBF-LB parts build with different orientations

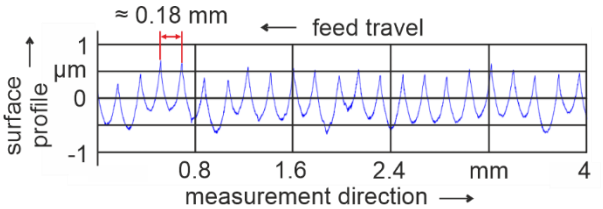

Figure 10: Representative surface profile

Such pores were created during the PBF-LB. They are exposed due to the material removal during milling. Even though a high density was achieved in the PBF-LB, formation of pores can never fully be eliminated [Snow 2020]. As surface pores may facilitate crack formation under load, a proper quality control of additively-subtractively manufactured parts is recommended in order to avoid a premature component failure.

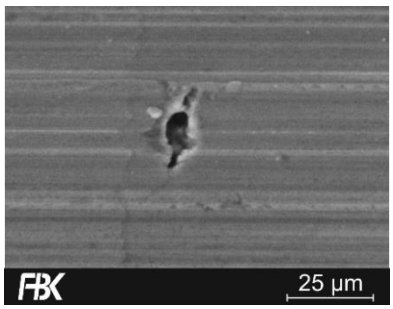

Figure 11: Example of pore on surface of PBF-LB material after milling

SEM micrographs of surfaces generated with different cutting conditions can be found in Figure 12. Grooves in the cutting direction of the end mill are visible on all surfaces. They represent the roughness of the cutting edge. A serrated structure is apparent for AM 0° parts milled with the lower cutting speed. For dry cutting, the serrated structure is less homogenous than for flood cooling, where it is more restricted to the individual grooves. The serrated structure looks similar to the "flakes" described in [Ramoni 2021] and [Zimmermann 2021] for face milling of PBF-LB

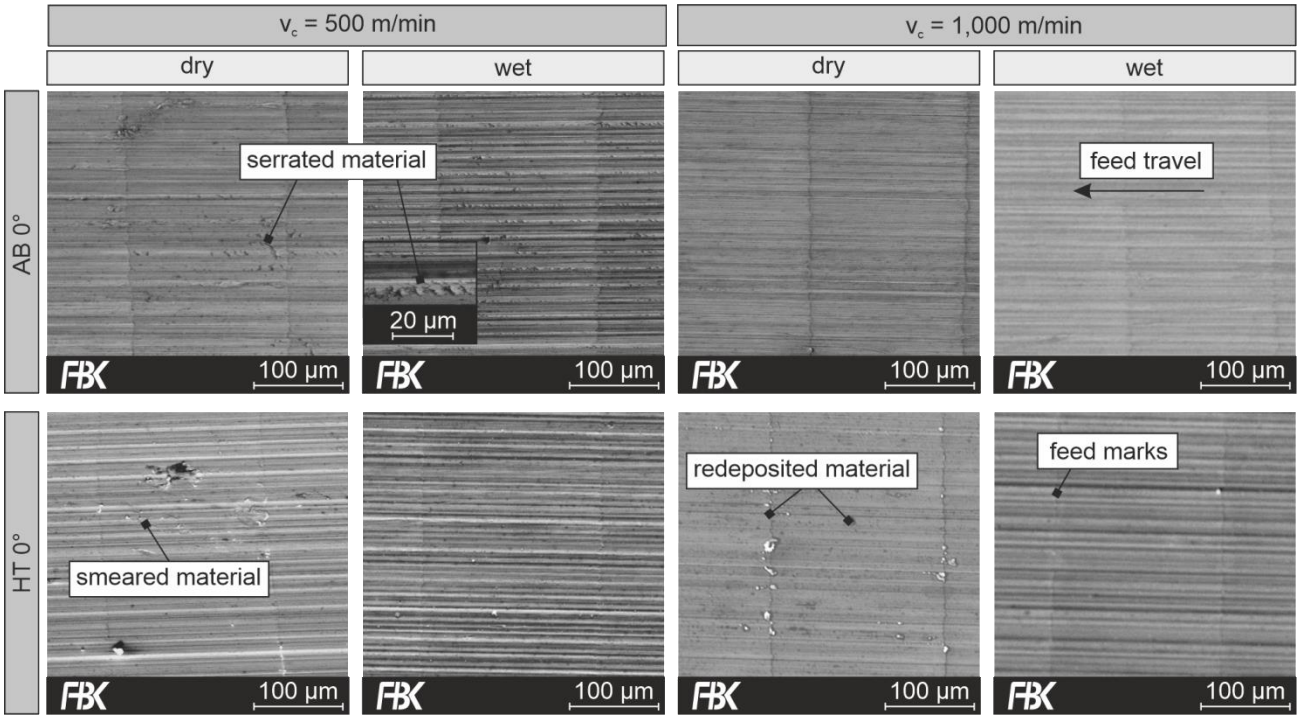

Figure 12: SEM images of differently milled surfaces

AlSi10Mg. The formation of the serrated structures described can be avoided by using high cutting speeds and by stress relieving the material (Figure 12). No serrated structures were formed in both cases. The formation of the serrated structure seems to be related to deformability of the AB material.

The use of metalworking fluid can decrease the amount of smeared and redeposited material on the milled surface. As discussed in the previous chapter, metalworking fluids decrease the friction between tool and workpiece material. The adhesion of workpiece or tool material on the machined surface that causes the redeposition is therefore reduced and less material is redeposited on the milled surface [Liao 2021]. Moreover, the plastic deformation of the surface appears to be reduced, as this mechanism leads to smearing. For the AB 0° parts, the influence of the metalworking fluid is particularly significant when using the smaller considered cutting speed. At the high cutting speed of v_c = 1,000 m/min, the milled surfaces of the AB 0° parts show only very low amounts of smeared or redeposited material for both dry and wet conditions.

Milling the heat treated parts results in more smeared and redeposited material on the surface than for the as-build parts when dry cutting. The microhardness is lower for heat treated parts and the microstructure is supposed to be slightly coarser due to the heat treatment. Therefore, the ductility of the heat treated material is higher. This facilitates the adhesion of material. Hence, the formation of build-up edges (BUE) and the redeposition of BUE material is more likely to occur. Images of the tools were taken with an optical microscope after each of 7 cuts (representing the end of use in this study). An image is depicted in Figure 13. Adhesions on the cutting edge are clearly visible. They have already partly detached from the cutting edge and would have been deposited on the surface if the tool had been further used. Concerning the heat treated parts, an increase of cutting speed does not have the same effect on the geometrical surface irregularities than for the as-built parts. At the surfaces of the heat-treated parts, redeposited material can still be found, despite the use of the maximum considered cutting speed.

4 SUMMARY

As-built parts and heat-treated AlSi10Mg parts were milled with different cutting conditions. The parts were manufactured with laser-based powder bed fusion (PBF-LB) in two building directions: 0° and 45°. The process forces during milling and the surface quality after milling were investigated in dependence of the manufacturing route of the material and the cutting condition.

The stress relief heat treatment reduced the microhardness of the PBF-LB material significantly by 16 % and partially dissolved the characteristic melt path borders in the materials microstructure. The built-up direction did not affect the microhardness. A clear impact of the stress relieving or the built-up direction on the process forces could not be found. Their influence on the process forces depends on the cutting condition used for milling. Milling improved the surface quality of the PBF-parts significantly. However, geometrical surface irregularities such as pores, smeared material or redeposited material were found on the milled surfaces. The surface porosity solely depends on the PBF-LB process and cannot be fully avoided. Smeared and redeposited material are a result of unsuitable cutting conditions. The lowest amount of surface irregularities on the surface was detected when using the highest cutting speed considered of 1,000 m/min and flood cooling. For milling AB PBF-LB parts, a good surface quality could also be achieved for dry cutting when applying a high cutting speed.

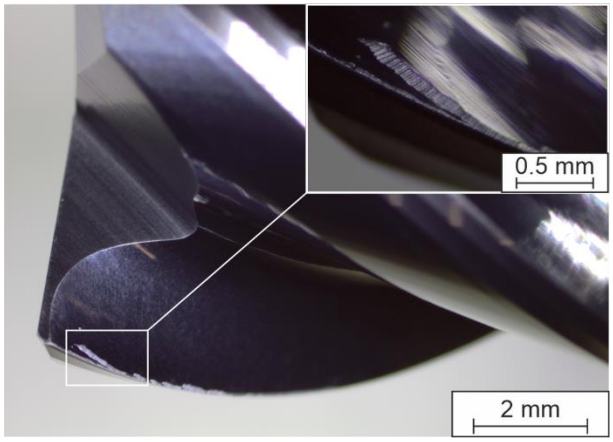

Figure 13: Cutting edge of tool with signs of adhesion

5 ACKNOWLEDGMENTS

This work was funded by KSB Foundation within the project "Gestaltung additiv-subtraktiver Prozessketten der Fertigung".

[1]Naming of specific manufacturers is done solely for the sake of completeness and does not necessarily imply an endorsement of the named companies nor that the products are necessarily the best for the purpose.

6 REFERENCES

[Aboulkhair 2019] Aboulkhair, N et al. (2019): 3D printing of Aluminium alloys: Additive Manufacturing of Aluminium alloys using selective laser melting. Progress in Materials Science 106, S. 100578.

[Alexeev 2017] Alexeev, V. et al. (2017): Influence of the direction of selective laser sintering on machinability of parts from 316L steel. IOP Conf. Ser.: Mater. Sci. Eng. 177, S. 12120.

[Bai 2021] Bai, Y. et al. (2021): Microstructure and machinability of selective laser melted high-strength maraging steel with heat treatment. Journal of Materials Processing Technology 288, S. 116906.

[Brinksmeier 2010] Brinksmeier, E et al. (2010): Surface integrity of selective-laser-melted components. CIRP Annals 59 (1), S. 601–606.

[Buchbinder 2013] Buchbinder, D. (2013): Selective Laser Melting von Aluminiumgusslegierungen. Zugl.: Aachen, Techn. Hochsch., Diss., 2013. Aachen: Shaker (Berichte aus der Lasertechnik).

[Calignano 2017] Calignano, F et al. (2017): Investigation of accuracy and dimensional limits of part produced in aluminum alloy by selective laser melting. Int J Adv Manuf Technol 88 (1-4), S. 451–458.

[Fernandez-Zelaia 2019] Fernandez-Zelaia et al. (2019): The effects of material anisotropy on secondary processing of additively manufactured CoCrMo. Additive Manufacturing 29, S. 100764.

[Fiocchi 2021] Fiocchi, J. et al. (2021): Heat treatment of aluminium alloys produced by laser powder bed fusion: A review. Materials & Design 204, S. 109651.

[Fortunato 2018] Fortunato, A. et al. (2018): Milling of maraging steel components produced by selective laser melting. Int J Adv Manuf Technol 94 (5-8), S. 1895–1902.

[Gebhardt 2013] Gebhardt, A. (2013): Generative Fertigungsverfahren. Additive Manufacturing und 3D Drucken für Prototyping - Tooling - Produktion. 1. Aufl. s.l.: Carl Hanser Fachbuchverlag.

[Grzesik 2019] Grzesik, W. and Rech, J. (2019): Influence of machining conditions on friction in metal cutting process – A review. Mechanik 92 (4), S. 242–248.

[Jarosz 2020] Jarosz, K. et al. (2020): Mechanistic force modeling in finish face milling of additively manufactured Inconel 625 nickel-based alloy. Int J Adv Manuf Technol 111 (5-6), S. 1535–1551.

[Kempen 2012] Kempen, K. et al. (2012): Mechanical Properties of AlSi10Mg Produced by Selective Laser Melting. Physics Procedia 39, S. 439–446.

[Kishawy 2005] Kishawy, H. A. et al. (2005): Effect of coolant strategy on tool performance, chip morphology and surface quality during high-speed machining of A356 aluminum alloy. International Journal of Machine Tools and Manufacture 45 (2), S. 219–227.

[Krüger 2014] Krüger, M. (2014): Modellbasierte Online-Bewertung von Fräsprozessen. Dissertation. Gottfried Wilhelm Leibniz Universität Hannover, Hannover.

[Leary 2017] Leary, M. (2017): Surface roughness optimisation for selective laser melting (SLM): Accommodating relevant and irrelevant surfaces. Laser Additive Manufacturing - Materials, Design, Technologies, and Applications, S. 99–118.

[Maamoun 2018] Maamoun, A. H. et al. (2018): Effect of Selective Laser Melting Process Parameters on the Quality of Al Alloy Parts: Powder Characterization, Density, Surface Roughness, and Dimensional Accuracy. Materials (Basel, Switzerland) 11 (12), S. 2343.

[Malakizadi 2022] Malakizadi, A. et al. (2022): Post-processing of additively manufactured metallic alloys – A review. International Journal of Machine Tools and Manufacture 179, S. 103908.

[Milton 2016] Milton, S. et al. (2016): Influence of Finish Machining on the Surface Integrity of Ti6Al4V Produced by Selective Laser Melting. Procedia CIRP 45, S. 127–130.

[Ming 2019] Ming, W. et al. (2019): Dynamic mechanical properties and machinability characteristics of selective laser melted and forged Ti6Al4V. Journal of Materials Processing Technology 271, S. 284–292.

[Liao 2021] Liao, Z. et al. : Surface integrity in metal machining - Part I: Fundamentals of surface characteristics and formation mechanisms. International Journal of Machine Tools and Manufacture 162, S.1-51.

[Neuenfeldt 2021] Neuenfeldt, M et al. (2021): Influence of LPBF process parameters on milling of a maraging tool steel. MM SJ 2021 (5), S. 5030–5037.

[Oliveira 2021] Oliveira, A. et al. (2021): Concurrent improvement of surface roughness and residual stress of as-built and aged additively manufactured maraging steel post-processed by milling. Int J Adv Manuf Technol 116 (7-8), S. 2309–2323.

[Ozcelik 2011] Ozcelik, B. et al. (2011): Comparison of Dry and Wet End Milling of AISI 316 Stainless Steel. Materials and Manufacturing Processes 26 (8), S. 1041–1049.

[Pérez-Ruiz 2021] Pérez-Ruiz, J. D. et al. (2021): On the relationship between cutting forces and anisotropy features in the milling of LPBF Inconel 718 for near net

shape parts. International Journal of Machine Tools and Manufacture 170, S. 103801.

[Piscopo 2019] Piscopo, G. et al. (2019): Machining induced residual stresses in AlSi10Mg component produced by Laser Powder Bed Fusion (L-PBF). Procedia CIRP 79, S. 101–106.

[Plocher 2019] Plocher, J. and Panesar, A. (2019): Review on design and structural optimisation in additive manufacturing: Towards next-generation lightweight structures. Materials & Design 183, S. 108164.

[Ramoni 2021] Ramoni, M. et al. (2021): An experimental investigation of hybrid manufactured SLM based Al-Si10-Mg alloy under mist cooling conditions. Journal of Manufacturing Processes 70, S. 225–235.

[Rao 2001] Rao, B. and Shin, Y.C. (2001): Analysis on high-speed face-milling of 7075-T6 aluminum using carbide and diamond cutters. International Journal of Machine Tools and Manufacture 41 (12), S. 1763–1781.

[Raus 2017] Raus, A. A. et al. (2017): Mechanical and physical properties of AlSi10Mg processed through selective laser melting. Proceedings of the 7th International Conference on Mechanical and Manufacturing Engineering, Sustainable Energy Towards Global Synergy. Jogjakarta, Indonesia, 1–3 August 2016: Author(s) (AIP Conference Proceedings), S. 20027.

[Read 2015] Read, N. et al. (2015): Selective laser melting of AlSi10Mg alloy: Process optimisation and mechanical properties development. Materials & Design (1980-2015) 65, S. 417–424.

[Růžičková 2022] Růžičková, L. et al. (2022): Influence of Stress Relief Annealing Parameters on Mechanical Properties and Decomposition of Eutectic Si Network of L-PBF Additive Manufactured Alloy AlSi10Mg. Metals 12 (9), S. 1497.

[Santos 2016] Santos, M. C. et al. (2016): Machining of aluminum alloys: a review. Int J Adv Manuf Technol 86 (9-12), S. 3067–3080.

[Schmidt 2022] Schmidt, M. et al. (2022): Support Structure Impact in Laser-Based Powder Bed Fusion of AlSi10Mg. Procedia CIRP 108, S. 88–93.

[Segebade 2019] Segebade, E. et al. (2019): Influence of anisotropy of additively manufactured AlSi10Mg parts on chip formation during orthogonal cutting. Procedia CIRP 82, S. 113–118.

[Snow 2020] Snow, Z. et al. (2020): Invited Review Article: Review of the formation and impact of flaws in powder bed fusion additive manufacturing. Additive Manufacturing 36, S. 101457.

[Sreejith 2008] Sreejith, P. S. (2008): Machining of 6061 aluminium alloy with MQL, dry and flooded lubricant conditions. In: Materials Letters 62 (2), S. 276–278. DOI: 10.1016/j.matlet.2007.05.019.

[Uzan 2017] Uzan, N. E. et al. (2017): Fatigue of AlSi10Mg specimens fabricated by additive manufacturing selective laser melting (AM-SLM). Materials Science and Engineering: A 704, S. 229–237.

[Wang 2018] Wang, L. et al. (2018): An approach to predict the residual stress and distortion during the selective laser melting of AlSi10Mg parts. Int J Adv Manuf Technol 97 (9-12), S. 3535–3546.

[Wei 2017] Wei, P. et al. (2017): The AlSi10Mg samples produced by selective laser melting: single track, densification, microstructure and mechanical behavior. Applied Surface Science 408, S. 38–50.

[Zedan 2013] Zedan, Y. et al. (2013): Effects of lubrication modes on part quality during drilling 6061-T6 aluminium alloy. IJMMM 13 (2/3), Artikel 53225, S. 231.

[Zimmermann 2021] Zimmermann, M. et al. (2021): Analysis of the machinability when milling AlSi10Mg additively manufactured via laser-based powder bed fusion. Int J Adv Manuf Technol, S. 1–17.